Dichotomic nature of spin and electronic fluctuations in FeSe

A. Glamazda,[1,2] P. Lemmens,[3,4] J. M. Ok,[5,6] Jun Sung Kim,[5,6] and K.-Y. Choi[1,*]

[1]*Department of Physics, Chung-Ang University, Seoul 156-756, Republic of Korea*

[2]*B. I. Verkin Institute for Low Temperature Physics and Engineering, NASU, 61103 Kharkiv, Ukraine*

[3]*Institute for Condensed Matter Physics, TU Braunschweig, 38106 Braunschweig, Germany*

[4]*Laboratory for Emerging Nanometrology (LENA), TU Braunschweig, 38106 Braunschweig, Germany*

[5]*Department of Physics, Pohang University of Science and Technology, Pohang 790-784, Korea*

[6]*Center for Artificial Low Dimensional Electronic Systems, Institute for Basic Science, Pohang 37673, Korea*

(Received 21 August 2018; revised manuscript received 9 January 2019; published 21 February 2019)

We report on the symmetry-dependent Raman scattering studies of a FeSe single crystal over a broad frequency range of 60−7000 cm^{-1}. Our experimental data feature abundant excitation spectra of phonon, spin, charge, and electronic degrees of freedom. The 207-cm^{-1} B_{1g} mode, involving the out-of-plane vibrations of the Fe ions, undergoes a large frequency shift by 14 cm^{-1} due to orbital-phonon coupling. The Raman spectra are well separated into strongly symmetry-dependent excitations at energies below 3000 cm^{-1} and weakly symmetry-dependent electron-hole excitations above 3000 cm^{-1}. This is taken as evidence for the coexistence of itinerant and localized spins. A prominent low-energy Raman response peaked at 531 cm^{-1} observed only in B_{2g} symmetry is interpreted in terms of coupled spin and charge quadrupole fluctuations. Our Raman results suggest that the dichotomic character of electrons together with the small energy scale involved in orbital ordering of the degenerated d_{xz} and d_{yz} orbitals promotes the intriguing physics of FeSe.

DOI: 10.1103/PhysRevB.99.075142

I. INTRODUCTION

The iron-chalcogenide FeSe represents an exceptional example of Fe-based superconductors and enables us to explore the intriguing interplay between electronic nematicity and superconductivity [1,2]. Originally, the nematic transition which breaks the C_4 lattice symmetry precedes an antiferromagnetic striped order at T_N in many Fe-based superconductors. Nonetheless, the magnitude of structural distortions is enhanced below T_N, implying a mutual coupling between structure and magnetism. In this spin-nematic scenario, spin fluctuations related to the striped phase make a distinction between two perpendicular in-plane directions, thereby inducing a tetragonal-to-orthorhombic transition [3–7].

Similarly to other iron-based systems, FeSe undergoes a nematic transition at $T_S = 90$ K on cooling, yet, unlike many other Fe-based materials, the nematic order is not accompanied by a $(\pi,0)$ antiferromagnetic order [8–11]. This poses a challenge to the prevailing view on the magnetic origin of the nematicity. Therefore, several alternative explanations for the mechanism behind this transition have been suggested. There exists some experimental evidence in favor of each view. This includes the spontaneous orbital ordering of the Fe's $3d_{xz}$ and $3d_{yz}$ orbitals [10–12], the quadrupolar order accompanying the nematic order [13,14], and the formation of a quantum paramagnet or quantum spin liquids due to strong frustration [15–17].

In addition, angle-resolved photoemission and quasiparticle interference studies in bulk FeSe give evidence for orbital-selective superconducting pairing, signaling a close link between the orbital/nematic order and superconductivity [18–23]. Despite the fact that there is no magnetic order in FeSe at ambient pressure, significant magnetic fluctuations are observed both around the stripe-type wave vector and around the Néel-type wave vector over a broad energy range of 0–220 meV [24–28]. Polarized pump-probe spectroscopy shows the persistence of nematic and magnetic fluctuations at least up to 200 K [29]. This together with a rapidly growing spectral weight of the low-energy magnetic fluctuations for temperatures below T_S indicates the intimate coupling between the magnetic fluctuations and the electronic structure [2,9,30–32].

There exist several earlier Raman works that report low-lying charge nematic fluctuations, phonon anomalies, and magnetic excitations, mainly focusing on characteristic features of the individual excitations [33–37]. Notwithstanding, a whole landscape of spin, charge, orbital, and phonon dynamics has remained elusive. Thus, a simultaneous probe of all possible types of collective excitations, covering a sufficiently wide energy range, is highly requested for a more complete understanding.

In this paper, we present polarization-resolved Raman scattering results in a broad energy range of 60−7000 cm^{-1}. We obtain a rich set of phonon, spin, charge, and electron-hole excitations, which show both a distinct symmetry dependence and a marked temperature evolution through the nematic transition. Our Raman results uncover a dual nature of magnetic excitations and intertwined couplings among all low-energy excitations, bringing about an outstanding physics of FeSe.

II. EXPERIMENTAL DETAILS

Single crystals of FeSe were grown using the KCl-$AlCl_3$ flux technique as described in Ref. [11]. For Raman

*kchoi@cau.ac.kr

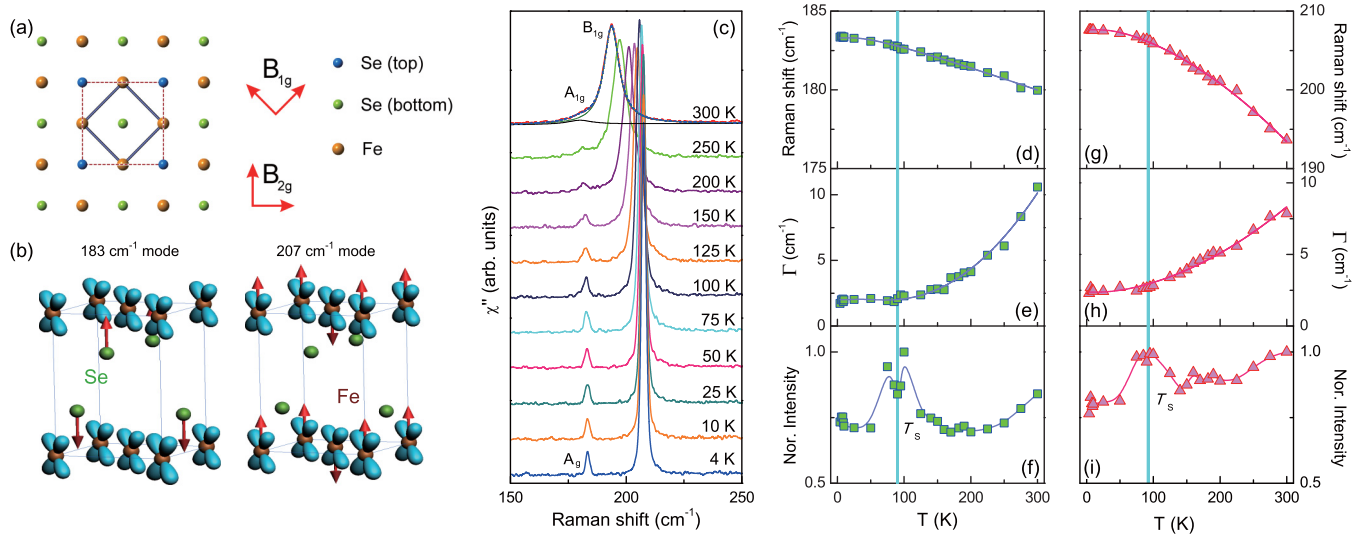

FIG. 1. (a) Sketch of the FeSe layer in the tetragonal phase composed of alternating Se atoms above and below the Fe plane. The solid blue (dashed brown) square represents the one (two)-Fe unit cell. The arrows denote the polarization directions of the incident and scattered light for the B_{1g} and B_{2g} symmetries. (b) Eigenvectors of the 183- and 207-cm^{-1} modes sketched together with d_{yz} orbitals. The related amplitude of the vibrations is represented by the length of the arrows. The brown (green) balls are the Fe (Se) atoms. (c) Temperature dependence of phonon modes recorded in the B_{1g} scattering channel. The solid lines at $T = 300$ K are the representative fits of the phonon peaks to a sum of Voigt profiles. Temperature dependence of (d) the frequency $\omega(T)$, (e) the full width at half maximum $\Gamma(T)$, and (f) the integrated intensity $I(T)$ for the 183-cm^{-1} A_{1g} mode. (g) $\omega(T)$, (h) $\Gamma(T)$, and (i) $I(T)$ for the 207-cm^{-1} B_{1g} mode. The solid lines in panels (d), (e), (g), and (h) are calculated curves following an anharmonic model as described in the text. The solid lines in panels (f) and (i) are guides to the eye.

scattering measurements, samples with typical dimensions of $1 \times 0.5 \times 0.2\,\text{mm}^3$ were cleaved parallel to the (110) plane to obtain fresh surfaces and installed into a He flow cryostat with a temperature range of $T = 4-300$ K. A laser beam ($\lambda = 532$ nm) was focused to a few-micrometer-diameter spot on the surface of the crystals using a 50-times-magnification microscope objective. The scattered spectra were dispersed and recorded by a micro-Raman spectrometer (Jobin Yvon, LabRam) equipped with a liquid-nitrogen-cooled CCD.

III. RESULTS AND DISCUSSION

A. Phonon anomalies

The high-T crystal phase of FeSe is described by the tetragonal $P4/nmm$ space group. Upon cooling through the nematic phase transition, the tetragonal symmetry is transformed into the orthorhombic $Cmma$ symmetry by a spontaneous breaking of the fourfold rotational symmetry. The orthorhombic unit cell is rotated by 45° with respect to the tetragonal one. Herein, we use x and y to assign tetragonal crystallographic axes and a and b for the orthorhombic axes which are rotated by 45° from the x and y axes, respectively.

According to the factor group analysis for the $P4/nmm$ space group, the total irreducible representation of Raman-active phonon modes above T_S is given by $\Gamma_{\text{Raman}} = A_{1g}(xx, yy, zz) + B_{1g}(xx, yy) + 2E_g(xz, yz)$. For temperatures below T_S, the factor group analysis for the $Cmma$ crystal symmetry yields in total six Raman-active modes: $\Gamma_{\text{Raman}} = A_g(aa, bb, cc) + B_{1g}(ab) + 2B_{2g}(ac) + 2B_{3g}(bc)$. For the symmetry-resolved probe of nematic charge fluctuations and magnetic excitations, we employ a frequently used scattering geometry sketched in Fig. 1(a). The B_{1g} (B_{2g}) symmetry is selectively detected using the cross-polarized incident and scattered light rotated by 45° (without rotation) with respect to the unit vectors of the tetragonal lattice.

We first identify key signatures of phonons by cooling through the nematic transition. Figure 1(c) presents the temperature-dependent Raman response of FeSe taken in the B_{1g} scattering configuration. Here, the Raman spectra are corrected by the Bose thermal factor $[1 - \exp(-\hbar\omega/k_B T)]$ to obtain the imaginary part of the Raman response function $\chi''(\omega)$.

At $T = 4$ K we observe two phonon peaks at 183 and 207 cm^{-1}. The intense peak at 207 cm^{-1} is assigned to the B_{1g} mode predicted by the factor group analysis. The weak, symmetry-forbidden 183-cm^{-1} mode, assigned to the A_g symmetry, may appear due to a small misalignment of the light polarizers with respect to the crystallographic axes. According to the correlation table, the A_g (B_{1g}) mode of the low-T orthorhombic phase is correlated with the A_{1g} (B_{1g}) mode of the high-T tetragonal phase.

With increasing temperature, the phonon modes significantly broaden and shift to lower frequency. Noticeably, there appear no new phonon modes through the structural phase transition, indicative of its subtle character. To detail the temperature evolution of phonon parameters, the Raman spectra are fitted to a sum of Voigt profiles. The latter profile is a convolution of a Gaussian function with a Lorentzian function where the Gaussian function is invoked due to the spectral resolution of Raman spectrometer and the Lorentzian function describes the phonon line broadening.

Shown in Figs. 1(d)–1(i) are the T dependencies of the extracted phonon frequencies $\omega(T)$, the full widths at half maximum (FWHM) $\Gamma(T)$, and the normalized intensities $I(T)$ for the 183- and 207-cm^{-1} modes. Upon heating from 4 to 300 K, the 183-cm^{-1} A_g mode, involving out-of-phase

TABLE I. List of parameters and constants for the anharmonic phonon-relaxation model.

Mode	ω_0	A	B	Γ_0	C	D
A_{1g}	184.1 cm^{-1}	−0.837	−0.009	3.8 cm^{-1}	−2.274	0.475
B_{1g}	209.3 cm^{-1}	−1.325	−0.383	1.7 cm^{-1}	0.504	0.162

vibrations of the Se atoms along the c axis, undergoes a softening by about 3.4 cm^{-1}, which is a typical value expected for lattice anharmonicities [see Fig. 1(b) for its normal-mode eigenvector]. In sharp contrast, the 207-cm^{-1} B_{1g} mode, involving out-of-phase out-of-plane vibrations of the Fe atoms, displays a huge and remarkable softening by 14 cm^{-1}. This effect is in accordance with the previous Raman result, which showed a similar softening by 13 cm^{-1} [33].

The mode-selective large frequency shift is ascribed to a phonon-orbital coupling. Upon cooling through the nematic transition, the degenerate d_{xz} and d_{yz} orbitals are split, thereby giving rise to an orbital order [20]. In consideration of symmetry, there is no distinction between the B_{1g} and A_{1g} phonon modes (having similar atomic displacements) in their biquadratic coupling to the nematic order parameter. As shown in Fig. 1(b), however, the B_{1g} (A_{1g}) mode involves only an iron (chalcogen) vibration. As a consequence, the B_{1g} mode is more strongly affected by the variation of the Fe orbitals than the A_{1g} mode. We recall that such a mode-specific huge phonon anomaly has been reported in the orbital-polaron manganite $La_{1-x}Sr_xMnO_3$, the spin-dimer system $Sr_3Cr_2O_8$, as well as in the spin-chain system $TiPO_4$ [38–40]. All these compounds commonly feature pronounced orbital fluctuations, which evolve to orbital ordering below room temperature. Thus, the observed large softening of the B_{1g} mode arises from the phonon energy renormalization via orbital-phonon coupling.

Further examining the phonon anomalies, the temperature evolution of $\omega(T)$ and $\Gamma(T)$ is described in terms of an anharmonic model including cubic and quartic phonon decay processes [41]:

$$\omega(T) = \omega_0 + A[1 + 2/(e^x - 1)] + B[1 + 3/(e^y - 1) + 3/(e^y - 1)^2], \quad (1)$$

$$\Gamma(T) = \Gamma_0 + C[1 + 2/(e^x - 1)] + D[1 + 3/(e^y - 1) + 3/(e^y - 1)^2], \quad (2)$$

where $x = \hbar\omega_0/2k_BT$, $y = \hbar\omega_0/3k_BT$, and A, B, C, and D are constants describing the three- and four-phonon decay processes. Here, ω_0 and Γ_0 are the bare frequency and the residual FWHM of the optical mode at $T = 0$ K, respectively. The fitting parameters are listed in Table I. This phonon anharmonic model seems to provide a reasonable description of the experimental data, as shown in the solid lines of Figs. 1(d)–1(h). Importantly, however, we find a significant contribution of the four-phonon process to the phonon FWHM and frequency for the 207-cm^{-1} mode, that is, $B/A = 0.289$ and $D/C = 0.321$. Even for the case of the 183-cm^{-1} mode, the negative value of C invalidates the anharmonic model.

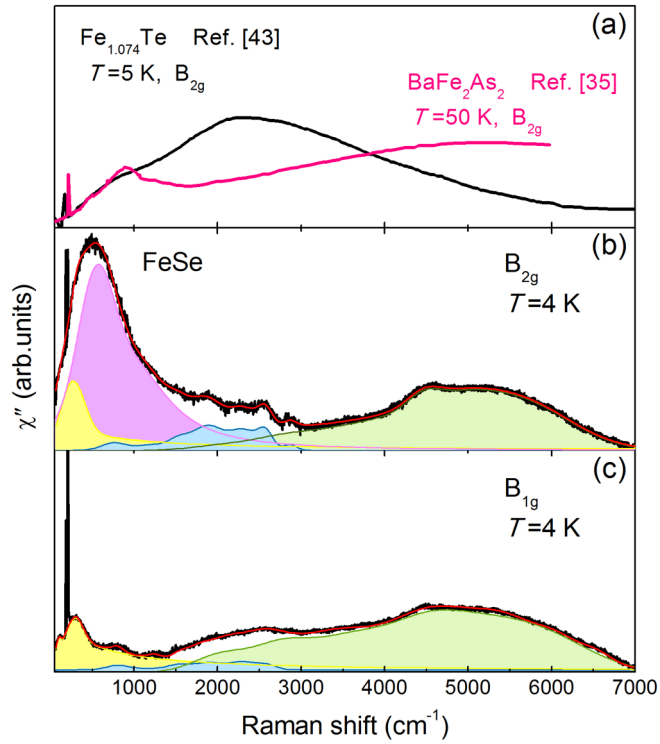

FIG. 2. (a) Raman response of $Fe_{1.074}Te$ and $BaFe_2As_2$ taken in the B_{2g} symmetry at $T = 5$ and 50 K, respectively. The data are taken from Refs. [35] and [43]. (b) Raman response of FeSe in the B_{2g} symmetry at $T = 4$ K. (c) Raman response of FeSe in the B_{1g} symmetry at $T = 4$ K. The colored shaded areas describe the decomposition of the Raman response into several components, including spin, charge, and electronic excitations as discussed in the text.

Overall, the phonons are subject to strong lattice anharmonicity due to the orbital fluctuations above T_S.

We next turn to the T dependence of the normalized intensities $I(T)$. As plotted in Figs. 1(f) and 1(i), $I(T)$ decreases and then forms a broad maximum at T_S with decreasing temperature. In insulating materials, $I(T)$ is determined by a change of a dielectric function with respect to the displacement of a normal mode or a modification of band energy. As the nematic transition accompanies the reconstruction of the electronic structure, the enhanced $I(T)$ through T_S is suggested to be related to a band reconstruction. The resemblance between $I(T)$ and $I_{QES}(T)$ [see below and Fig. 3(b)], reflecting a d-wave Pomeranchuk instability of the Fermi surface, lends further support to this conclusion [34]. In contrast to $I(T)$, no discernible changes are detected for $\omega(T)$ and $\Gamma(T)$ at T_S, suggesting a delicate nature of the Fermi surface reconstruction.

B. Magnetic excitations

Figure 2 compares the $T = 4$ K $\chi''(\omega)$ of FeSe between the B_{1g} and B_{2g} symmetry channels in the wide frequency region of 60−7000 cm^{-1} (∼7−868 meV) along with the $T = 5$ K $Fe_{1.074}Te$ and $T = 50$ K $BaFe_2As_2$ data. We recall that the previous Raman investigations were limited to an energy below 3600 cm^{-1}. Our high-energy data extending to 7000 cm^{-1}

convey key information about the underlying nature of diverse excitations.

As shown in Figs. 2(b) and 2(c), we observe a strongly symmetry-dependent $\chi''(\omega)$ in the frequency range up to approximately 3000 cm^{-1} and a weakly symmetry-dependent $\chi''(\omega)$ in the higher-frequency range of 3000−7000 cm^{-1}. The high-frequency excitations (yellowish green shadings) above 3000 cm^{-1} are assigned to an electron-hole continuum, judging from their weak polarization dependence and the comparison to the $BaFe_2As_2$ spectrum. In the energy range up to approximately 3000 cm^{-1}, the B_{2g} symmetry shows a prominent scattering cross section that stems from several components. Following the previous assignment of Massat *et al.* [34], the low-energy quasielastic response (yellow shadings) is ascribed to the ferroquadrupole fluctuations of a d-wave Pomeranchuk instability and is phenomenologically modeled by a Drude function $\chi''_{QES}(\omega, T) \propto \omega\Gamma/(\omega^2 + \Gamma^2)$, where Γ is the carrier scattering rate. An asymmetry maximum centered at 531 cm^{-1} (purple shading) was controversially interpreted in terms of stripe quadrupole fluctuations or two-magnon Raman scattering [35,36]. In addition, there are residual contributions (cadet blue shadings) in the intermediate frequency range of 500−3000 cm^{-1}, which may be composed of remaining weak electron-hole and spin excitations or of interband electronic excitations [42].

To separate each component from the total spectrum, we first fit the quasielastic signal to the above Drude function in the B_{1g} symmetry where the two-magnon signal is negligible [see Fig. 2(c)]. Next, the predetermined quasielastic contribution in the B_{1g} channel is scaled to obtain a smooth spectral shape of the two-magnon scattering in the B_{2g} channel. As precise functional forms of the spin excitations are not known, the lower-energy two-magnon and higher-energy excitation spectra are approximated by a sum of multiple Lorentzian lines. The resulting decomposition is marked by color shadings in Figs. 2(b) and 2(c).

To gain further insight into the assignments of $\chi''(\omega)$, the Raman response of FeSe is compared to that of $BaFe_2As_2$ and $Fe_{1.074}Te$. The Raman data of $BaFe_2As_2$ and $Fe_{1.074}Te$ presented in Fig. 2(a) are taken from Refs. [35,43]. Although Fe(Se, Te) is a metal with itinerant electrons, there is experimental and theoretical evidence that its low-energy physics is well captured by localized electrons [44,45]. $Fe_{1.074}Te$ exhibits a broad maximum at $\omega_p = 2300\ cm^{-1}$ with a low-energy shoulder at 860 cm^{-1}, extending to an energy of $\omega_{cutoff} = 6500\ cm^{-1}$. The well-defined peak is typical for two-magnon excitations occurring through double spin-flip processes within the Fleury-Loudon formulation for Heisenberg-type exchange interactions between the localized spins [43,46]. Compared to $Fe_{1.074}Te$, $BaFe_2As_2$, which is more weakly correlated than $Fe_{1.074}Te$, exhibits a much broader bandwidth with a low-energy peak at about 900 cm^{-1} and a high-energy featureless maximum at approximately 5000 cm^{-1}, corresponding to the formation of a $(\pi,0)$ spin-density wave and an electron-hole continuum, respectively.

Generically, the spectral form, the polarization dependence, and the peak energy of magnetic Raman excitations depend on a nature of magnetic moments and magnetic exchange interactions of a system. In this regard, the featureless maximum observed in $BaFe_2As_2$ is linked to the $(\pi,0)$ spin fluctuations of a rather itinerant character. With this in mind, we take a close look at $\chi''(\omega)$ of FeSe. We find that its Raman spectrum is well separated into a lower-energy excitation part below 3000 cm^{-1} and a higher-energy excitation above 3000 cm^{-1}. It is remarkable that the high-energy excitation resembles $\chi''(\omega)$ of $BaFe_2As_2$ with regard to the spectral shape and peak energy. The weak polarization dependence in addition to these confirms its more itinerant character. The pronounced low-energy excitation peak at $\omega_p = 531\ cm^{-1}$ is reminiscent of the two-magnon excitation of $Fe_{1.074}Te$ with a well-defined peak at $\omega_p = 2300\ cm^{-1}$. The strong support for the two-magnon interpretation is provided by its marked polarization dependence between the B_{1g} and B_{2g} scattering channels. We further note that the well-defined two-magnon excitation does not necessarily require a long-range magnetic order unlike the one-magnon mode. As the hole-doped high-T_c cuprates show, the two-magnon peak is well preserved even in the presence of short-range spin fluctuations [47]. A dual character of the spin excitations is not unexpected because the (π,π) Néel-type and the $(\pi,0)$ stripe-type spin fluctuations coexist in FeSe [26]. The competing spin fluctuations can be taken as a signature for strong frustration, which leads to the strong reduction of the peak energy in FeSe, compared to $Fe_{1.074}Te$ [48]. We conclude that the two energetically distinct excitations are associated with the existence of more delocalized and localized orbitals, corresponding to itinerant and localized spin excitations.

In the pursuit of the two-magnon interpretation, the temperature evolution of the prominent low-energy excitation $\chi''_{2M}(\omega)$ with a peak of $\omega_p = 531\ cm^{-1}$ in the B_{2g} symmetry is detailed in Fig. 3(a). Here we note that $\chi''_{2M}(\omega)$ is obtained

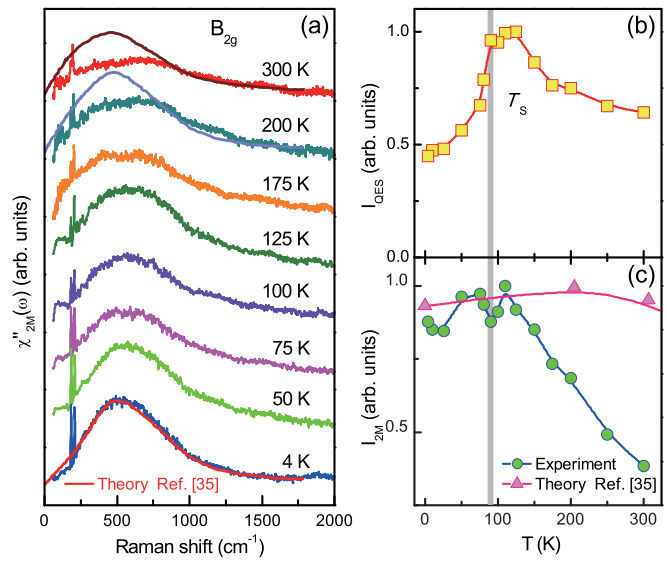

FIG. 3. (a) Temperature dependence of the putative two-magnon Raman response $\chi''_{2M}(\omega)$, obtained after subtracting the electronic and charge contributions. The data are shifted vertically for clarity. The overlaid solid lines are the calculated and scaled two-magnon Raman spectra from Ref. [35]. (b) Integrated intensity of the quasielastic response as a function of temperature, $I_{QES}(T)$. (c) Temperature evolution of the integrated intensity of the theoretical (pink triangles) and experimental (green circles) $\chi''_{2M}(\omega)$ data.

by a subtraction of $\chi''_{\rm QES}(\omega)$ and charge and electronic contributions in the frequency range $\omega = 60-2000\,{\rm cm}^{-1}$. In the multicomponent decomposition of $\chi''(\omega)$ we cannot completely exclude some uncertainty. For a cross-check of the decomposition procedure, we plot the integrated intensity of $\chi''_{\rm QES}(\omega)$, $I_{\rm QES}(T)$, in Fig. 3(b). Upon cooling towards $T_{\rm S}$, $I_{\rm QES}(T)$ shows a steady increase, forming its maximum intensity at about $T_{\rm S}$, and then drops rapidly. As $I_{\rm QES}(T)$ is associated with the nematic susceptibility, the critical-like enhancement at about $T_{\rm S}$ validates the adopted procedure [34].

Within a local magnetic moment picture, the low-energy physics of FeSe is captured by the $s = 1$ $J_1 - J_2 - J_3 - K$ Heisenberg model where the biquadratic term K tunes quantum fluctuations [15,16,35,48]. In the phase diagram of the $J_1 - J_2 - J_3 - K$ model FeSe lies in the intermediate coupling region ($J_2/J_1 \approx 0.525-0.555$), featuring the strong frustration. This model parameter gives an explanation of the gapped stripe and Néel spin fluctuations [15]. Baum *et al.* [35] takes a set of of the magnetic parameters ($J_2 = 0.528\,J_1$, $J_3 = 0$, and $K = 0.1\,J_1$) to compute two-magnon Raman scattering. Considering the technical difficulty of calculating two-magnon Raman spectra, it is beyond of the scope of the present work to determine the spin Hamiltonian by fitting our data. Instead, we compare our $T = 4$ K data with the numerically calculated $\chi''_{\rm 2M}(\omega)$ [three solid lines in Fig. 3(a)]. In this case, the free parameter is the exchange coupling constant J_1 that can be evaluated by the peak energy relation $\omega_{\rm p} \approx 0.3\,J_1$ [35]. We reach a good match between the theoretical and experimental data with the value of $J_1 = 221$ meV. It is noteworthy that the energy scale of J_1 is comparable to the high-energy cutoff of spin excitations observed by neutron scattering measurements [26]. However, the value of $J_1 = 221$ meV estimated by the magnetic Raman response is 1.8 times larger than $J_1 = 123$ meV calculated using *ab initio* density functional theory [16]. We recall that the peak energy is given by a function of the ratio J_2/J_1. When J_2/J_1 deviates away from 0.5, the peak energy shifts to higher energy [48]. Thus, $J_1 = 221$ meV puts an upper limit on the nearest-neighbor exchange constant.

Unlike the $T = 4$ K $\chi''_{\rm 2M}(\omega)$ data, a discrepancy between experiment and theory becomes sizable at high temperatures. In Fig. 3(c), we plot the integrated intensity of $\chi''_{\rm 2M}(\omega)$, $I_{\rm 2M}(T)$, vs temperature along with the theoretical data taken from Ref. [35]. With increasing temperature towards $T_{\rm S}$, $I_{\rm 2M}(T)$ tends to increase slightly and then shows a marked decrease above 100 K. This is in sharp contrast to the calculated data that show little change up to room temperature [pink triangles in Fig. 3(c)]. Given the large energy scale of $J_1 = 221$ meV $= 2564$ K, it is no wonder that the calculated $\chi''_{\rm 2M}(\omega)$ undergoes no appreciable thermal damping and renormalization of the magnetic fluctuations up to room temperature. This apparent inconsistency does not necessarily mean the failure of the two-magnon scenario. Noteworthy is that the splitting energy of 50 meV between the d_{yz} and d_{xz} orbitals is comparable to the peak energy of $\omega_{\rm p} = 531\,{\rm cm}^{-1}$ [49,50]. Thus, the orbital fluctuations above $T_{\rm S}$ provide a relaxation channel, leading to the drastic suppression of $I_{\rm 2M}(T)$. Another explanation is invoked by the correlation between the stripe-type spin and quadrupole charge fluctuations [36]. In this case, $\chi''_{\rm 2M}(\omega)$ may attain a hybrid nature of spin and charge excitations.

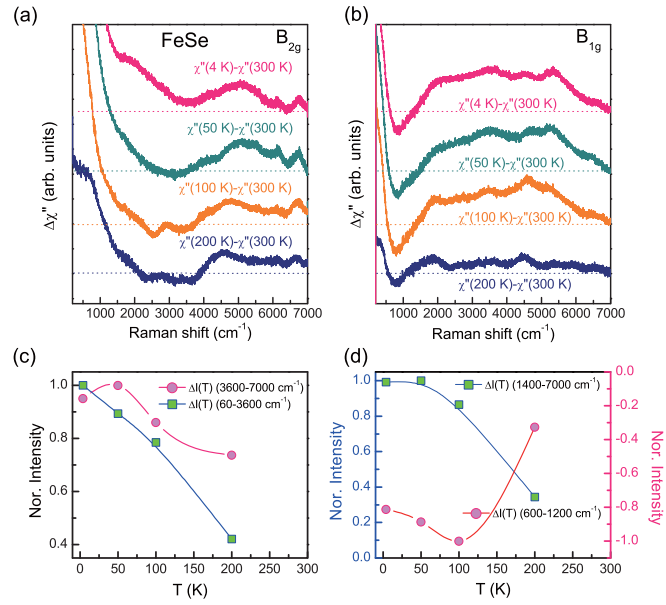

FIG. 4. Temperature evolution of subtracted spectra $\Delta\chi''(T) = \chi''(T) - \chi''(300\,{\rm K})$ (a) in B_{2g} symmetry and (b) in B_{1g} symmetry. The data are vertically shifted for clarity. Temperature dependence of the integrated $\Delta\chi''(T)$ for the lower- and higher-frequency intervals (c) in B_{2g} symmetry and (d) in B_{1g} symmetry, respectively.

Lastly, we have a closer look at the temperature evolution of $\chi''(T,\omega)$ over the entire measured frequency range. To highlight the small spectral redistribution, we plot the subtracted spectra $\Delta\chi''(T,\omega) = \chi''(T,\omega) - \chi''(300\,{\rm K},\omega)$ vs temperature in Figs. 4(a) and 4(b) for the B_{2g} symmetry and the B_{1g} symmetry, respectively. In the B_{2g} symmetry, upon cooling from 200 K, $\Delta\chi''(T,\omega)$ increases appreciably below $3600\,{\rm cm}^{-1}$, while changing a spectral form above $3600\,{\rm cm}^{-1}$. This is contrasted with the B_{1g} symmetry's $\Delta\chi''(T,\omega)$, which shows an increase of the spectral depletion between 600 and $1200-1400\,{\rm cm}^{-1}$ and an enhanced spectral weight above $1400\,{\rm cm}^{-1}$.

For a quantification of this trend, we present the temperature dependence of the integrated $\Delta\chi''(T,\omega)$, $\Delta I(T,[\omega_1,\omega_2]) = \int_{\omega_1}^{\omega_2}\Delta\chi''(T,\omega)d\omega$, in the two different frequency intervals in Figs. 4(c) and 4(d). In the B_{2g} symmetry, $\Delta I(T,[600\,{\rm cm}^{-1}, 3600\,{\rm cm}^{-1}])$ displays a more rapid increase than $\Delta I(T,[3600\,{\rm cm}^{-1}, 7000\,{\rm cm}^{-1}])$ with decreasing temperature. In the B_{1g} symmetry, $\Delta I(T,[600\,{\rm cm}^{-1}, 1200\,{\rm cm}^{-1}])$ exhibits a steep increase up to 100 K and then a small drop upon further cooling to 4 K, while $\Delta I(T,[1400\,{\rm cm}^{-1}, 7000\,{\rm cm}^{-1}])$ is in parallel with the B_{2g} symmetry's $\Delta I(T,[600\,{\rm cm}^{-1}, 3600\,{\rm cm}^{-1}])$. The evolution of the depleted spectral weight in the B_{1g} symmetry with temperature indicates a gap opening in some part of the Fermi surface.

IV. CONCLUSION

Polarization-resolved Raman spectroscopy has been employed to elucidate the nature of phonon, spin, charge, and

orbital dynamics and their mutual couplings in FeSe. The sufficiently wide frequency range of $60-7000\,\mathrm{cm}^{-1}$ of our data enables us to probe and distinguish all possible types of collective excitations. Our results show a large degree of consistency with the phonon, spin, charge, and electron excitations previously reported in the literature [33–36]. The salient point of the present study is the energy separation observed into strongly symmetry-dependent excitations below $3000\,\mathrm{cm}^{-1}$ and a weakly symmetry-dependent electron-hole continuum above $3000\,\mathrm{cm}^{-1}$. This gives compelling evidence for a coexistence of itinerant and localized spins and electrons. In addition, there are experimental signatures that phonon, spin, charge, and orbital dynamics are intimately tied.

First, we observe a large and mode-specific softening of the 207-cm^{-1} B_{1g} mode by 14 cm^{-1} ascribed to orbital-phonon coupling and in accordance with the out-of-plane Fe vibrations of this mode.

Second, the prominent low-energy Raman response $\chi''_{2\mathrm{M}}(\omega)$ peak at $531\,\mathrm{cm}^{-1}$ is observed only in B_{2g} symmetry. The $T = 4$ K $\chi''_{2\mathrm{M}}(\omega)$ data are well reproduced by the $J_1 - J_2 - K$ Heisenberg spin Hamiltonian with the magnetic parameters $J_1 = 221$ meV and $J_2 = 0.528\,J_1$ and $K = 0.1\,J_1$. However, this two-magnon assignment is questionable due to the rapid suppression of its scattering intensity for temperatures above T_S. One probable account for this inconsistency is made by a coupling of the stripe spin and quadrupole charge fluctuations.

Third, the intensities of phonons, quasielastic response, and two-magnon scattering as a function of temperature bear resemblance to a broad maximum at T_S. This suggests that the lattice, spin, and nematic dynamics are correlated to the Fermi surface reconstruction.

In conclusion, FeSe occupies a special position among the Fe-based superconductors thanks to a dichotomic nature of involved orbitals and their orbital ordering. The involved small-energy scales together with the anisotropy in the Brillouin zone induce an intertwined coupling of lattice, magnetic, and structural degrees of freedom and, on the other hand, features competing spin and electronic fluctuations.

ACKNOWLEDGMENTS

This work was supported by the Korea Research Foundation (KRF) (Grants No. 2018-0189 and No. 2018-0099), DFG Grant No. RTG 1953/1, Metrology for Complex Nanosystems, and DFG Grant No. LE967/16-1. The work at POSTECH was supported by the National Research Foundation (NRF) of Korea through the SRC (No. 2018R1A5A6075964) and the Max Planck-POSTECH Center for Complex Phase Materials in Korea (MPK) (No. 2016K1A4A4A01922028).

[1] X. Liu, L. Zhao, S. He, J. He, D. Liu, D. Mou, B. Shen, Y. Hu, J. Huang, and X. J. Zhou, J. Phys.: Condens. Matter **27**, 183201 (2015).
[2] A. Böhmer and A. Kreisel, J. Phys.: Condens. Matter **30**, 023001 (2018).
[3] C. Fang, H. Yao, W.-F. Tsai, J. P. Hu, and S. A. Kivelson, Phys. Rev. B **77**, 224509 (2008).
[4] R. M. Fernandes, A. V. Chubukov, J. Knolle, I. Eremin, and J. Schmalian, Phys. Rev. B **85**, 024534 (2012).
[5] R. M. Fernandes and J. Schmalian, Supercond. Sci. Technol. **25**, 084005 (2012).
[6] R. M. Fernandes, A. V. Chubukov, and J. Schmalian, Nat. Phys. **10**, 97 (2014).
[7] A. V. Chubukov, M. Khodas, and R. M. Fernandes, Phys. Rev. X **6**, 041045 (2016).
[8] F.-C. Hsu, J.-Y. Luo, K.-W. Yeh, T.-K. Chen, T.-W. Huang, P. M. Wu, Y.-C. Lee, Y.-L. Huang, Y.-Y. Chu, D.-C. Yan, and M.-K. Wu, Proc. Natl. Acad. Sci. USA **105**, 14262 (2008).
[9] T. M. McQueen, A. J. Williams, P. W. Stephens, J. Tao, Y. Zhu, V. Ksenofontov, F. Casper, C. Felser, and R. J. Cava, Phys. Rev. Lett. **103**, 057002 (2009).
[10] A. E. Böhmer, T. Arai, F. Hardy, T. Hattori, T. Iye, T. Wolf, H. v. Löhneysen, K. Ishida, and C. Meingast, Phys. Rev. Lett. **114**, 027001 (2015).
[11] S.-H. Baek, D. V. Efremov, J. M. Ok, J. S. Kim, J. van den Brink, and B. Büchner, Nat. Mater. **14**, 210 (2015).
[12] S.-H. Baek, D. V. Efremov, J. M. Ok, J. S. Kim, Jeroen van den Brink, and B. Büchner, Phys. Rev. B **93**, 180502(R) (2016).
[13] R. Yu and Q. Si, Phys. Rev. Lett. **115**, 116401 (2015).
[14] Z. Wang, W.-J. Hu, and A. H. Nevidomskyy, Phys. Rev. Lett. **116**, 247203 (2016).
[15] F. Wang, S. A. Kivelson, and D. H. Lee, Nat. Phys. **11**, 959 (2015).
[16] J. K. Glasbrenner, I. I. Mazin, H. O. Jeschke, P. J. Hirschfeld, R. M. Fernandes, and R. Valenti, Nat. Phys. **11**, 953 (2015).
[17] J.-H. She, M. J. Lawler, and E.-A. Kim, Phys. Rev. Lett. **121**, 237002 (2018).
[18] K. Nakayama, Y. Miyata, G. N. Phan, T. Sato, Y. Tanabe, T. Urata, K. Tanigaki, and T. Takahashi, Phys. Rev. Lett. **113**, 237001 (2014).
[19] S. Mukherjee, A. Kreisel, P. J. Hirschfeld, and B. M. Andersen, Phys. Rev. Lett. **115**, 026402 (2015).
[20] A. I. Coldea and M. D. Watson, Annu. Rev. Condens. Matter Phys. **9**, 125 (2018).
[21] P. O. Sprau, A. Kostin, A. Kreisel, A. E. Böhmer, V. Taufour, P. C. Canfield, S. Mukherjee, P. J. Hirschfeld, B. M. Andersen, and J. C. S. Davis, Science **357**, 75 (2017).
[22] H. C. Xu, X. H. Niu, D. F. Xu, J. Jiang, Q. Yao, Q. Y. Chen, Q. Song, M. Abdel-Hafiez, D. A. Chareev, A. N. Vasiliev, Q. S. Wang, H. L. Wo, J. Zhao, R. Peng, and D. L. Feng, Phys. Rev. Lett. **117**, 157003 (2016).
[23] J. Kang, R. M. Fernandes, and A. Chubukov, Phys. Rev. Lett. **120**, 267001 (2018).
[24] S. Shamoto, K. Matsuoka, R. Kajimoto, M. Ishikado, Y. Yamakawa, T. Watashige, S. Kasahara, M. Nakamura, H. Kontani, T. Shibauchi, and Y. Matsuda, arXiv:1511.04267.

[25] Q. Wang, Y. Shen, B. Pan, Y. Hao, M. Ma, F. Zhou, P. Steffens, K. Schmalzl, T. R. Forrest, M. Abdel-Hafiez, X. Chen, D. A. Chareev, A. N. Vasiliev, P. Bourges, Y. Sidis, H. Cao, and J. Zhao, Nat. Mater. **15**, 159 (2016).

[26] Q. Wang, Y. Shen, B. Pan, X. Zhang, K. Ikeuchi, K. Iida, A. D. Christianson, H. C. Walker, D. T. Adroja, M. Abdel-Hafiez, X. Chen, D. A. Chareev, A. N. Vasiliev, and J. Zhao, Nat. Commun. **7**, 12182 (2016).

[27] M. C. Rahn, R. A. Ewings, S. J. Sedlmaier, S. J. Clarke, and A. T. Boothroyd, Phys. Rev. B **91**, 180501(R) (2015).

[28] M. Ma, P. Bourges, Y. Sidis, Y. Xu, S. Li, B. Hu, J. Li, F. Wang, and Y. Li, Phys. Rev. X **7**, 021025 (2017).

[29] C.-W. Luo, P. C. Cheng, S.-H. Wang., J.-C. Chiang, J.-Y. Lin, K.-H. Wu, J.-Y. Juang, D. A. Chareev, O. S. Volkova, and A. N. Vasiliev, npj Quantum Mater. **2**, 32 (2017).

[30] S. Kasahara, T. Watashige, T. Hanaguri, Y. Kohsaka, T. Yamashita, Y. Shimoyama, Y. Mizukami, R. Endo, H. Ikeda, K. Aoyama, T. Terashima, S. Uji, T. Wolf, H. von Lohneysen, T. Shibauchi, and Y. Matsuda, Proc. Natl. Acad. Sci. USA **111**, 16309 (2014).

[31] S. Onari, Y. Yamakawa, and H. Kontani, Phys. Rev. Lett. **116**, 227001 (2016).

[32] Y. Sun, S. Pyon, and T. Tamegai, Phys. Rev. B **93**, 104502 (2016).

[33] V. Gnezdilov, Y. G. Pashkevich, P. Lemmens, D. Wulferding, T. Shevtsova, A. Gusev, D. Chareev, and A. Vasiliev, Phys. Rev. B **87**, 144508 (2013).

[34] P. Massat, D. Farina, I. Paul, S. Karlsson, P. Strobel, P. Toulemonde, M.-A. Masson, M. Cazayous, A. Sacuto, S. Kasahara, T. Shibauchi, Y. Matsuda, and Y. Gallais, Proc. Natl. Acad. Sci. USA **113**, 9177 (2016).

[35] A. Baum, H. N. Ruiz, N. Lazarević, Y. Wang, T. Böhm, R. Hosseinian Ahangharnejhad, P. Adelmann, T. Wolf, Z. V. Popović, B. Moritz, T. P. Devereaux, and R. Hackl, Comms. Phys. **2**, 14 (2019).

[36] W.-L. Zhang, S.-F. Wu, S. Kasahara, T. Shibauchi, Y. Matsuda, and G. Blumberg, arXiv:1710.09892.

[37] P. Massat, Y. Quan, R. Grasset, M.-A. Méasson, M. Cazayous, A. Sacuto, S. Karlsson, P. Strobel, P. Toulemonde, Z. Yin, and Y. Gallais, Phys. Rev. Lett. **121**, 077001 (2018).

[38] K.-Y. Choi, P. Lemmens, T. Sahaoui, G. Güntherodt, Yu. G. Pashkevich, V. P. Gnezdilov, P. Reutler, L. Pinsard-Gaudart, B. Büchner, and A. Revcolevschi, Phys. Rev. B **71**, 174402 (2005).

[39] D. Wulferding, P. Lemmens, K.-Y. Choi, V. Gnezdilov, Y. G. Pashkevich, J. Deisenhofer, D. Quintero-Castro, A. T. M. Nazmul Islam, and B. Lake, Phys. Rev. B **84**, 064419 (2011).

[40] D. Wulferding, A. Möller, K.-Y. Choi, Y. G. Pashkevich, R. Yu. Babkin, K. V. Lamonova, P. Lemmens, J. M. Law, R. K. Kremer, and R. Glaum, Phys. Rev. B **88**, 205136 (2013).

[41] M. Balkanski, R. F. Wallis, and E. Haro, Phys. Rev. B **28**, 1928 (1983).

[42] H.-I. Hsiung, W. H. Chao, H. Y. Hsu, M.-J. Wang, H.-L. Liu, and M.-K. Wu, Physica C (Amsterdam, Neth.) **552**, 61 (2018).

[43] K. Okazaki, S. Sugai, S. Niitaka, and H. Takagi, Phys. Rev. B **83**, 035103 (2011).

[44] A. Tamai, A. Y. Ganin, E. Rozbicki, J. Bacsa, W. Meevasana, P. D. C. King, M. Caffio, R. Schaub, S. Margadonna, K. Prassides, M. J. Rosseinsky, and F. Baumberger, Phys. Rev. Lett. **104**, 097002 (2010).

[45] Z. P. Yin, K. Haule, and G. Kotliar, Nat. Mater. **10**, 932 (2011).

[46] P. A. Fleury and R. Loudon, Phys. Rev. **166**, 514 (1968).

[47] S. Sugai, H. Suzuki, Y. Takayanagi, T. Hosokawa, and N. Hayamizu, Phys. Rev. B **68**, 184504 (2003).

[48] H. Ruiz, Y. Wang, B. Moritz, and T. P. Devereaux, arXiv:1812.09609.

[49] T. Shimojima, Y. Suzuki, T. Sonobe, A. Nakamura, M. Sakano, J. Omachi, K. Yoshioka, M. Kuwata-Gonokami, K. Ono, H. Kumigashira, A. E. Bohmer, F. Hardy, T. Wolf, C. Meingast, H. V. Lohneysen, H. Ikeda, and K. Ishizaka, Phys. Rev. B **90**, 121111(R) (2014).

[50] P. Zhang, T. Qian, P. Richard, X. P. Wang, H. Miao, B. Q. Lv, B. B. Fu, T. Wolf, C. Meingast, X. X. Wu, Z. Q. Wang, J. P. Hu, and H. Ding, Phys. Rev. B **91**, 214503 (2015).